Calcif Tissue Int (2014) 94:248–257
DOI 10.1007/s00223-013-9806-7

ORIGINAL RESEARCH

Strontium Localization in Bone Tissue Studied by X-Ray Absorption Spectroscopy

Christian Grundahl Frankær · Anders Christer Raffalt · Kenny Stahl

Received: 1 August 2013 / Accepted: 16 September 2013 / Published online: 8 October 2013

Abstract Strontium has recently been introduced as a pharmacological agent for the treatment and prevention of osteoporosis. We determined the localization of strontium incorporated into bone matrix from dogs treated with Sr malonate by X-ray absorption spectroscopy. A new approach for analyzing the X-ray absorption spectra resulted in a compositional model and allowed the relative distribution of strontium in the different bone components to be estimated. Approximately 35–45 % of the strontium present is incorporated into calcium hydroxyapatite (CaHA) by substitution of some of the calcium ions occupying highly ordered sites, and at least 30 % is located at less ordered sites where only the first solvation shell is resolved, suggesting that strontium is surrounded by only oxygen atoms similar to Sr^{2+} in solution. Strontium was furthermore shown to be absorbed in collagen in which it obtains a higher structural order than when present in serum but less order than when it is incorporated into CaHA. The total amount of strontium in the samples was determined by inductively coupled plasma mass spectrometry, and the amount of Sr was found to increase with increasing dose levels and treatment periods, whereas the relative distribution of strontium among the different components appears to be independent of treatment period and dose level.

Keywords Strontium malonate · X-ray absorption spectroscopy · Apatite · Dog bone · Strontium incorporation

Christian Grundahl Frankær, Anders Christer Raffalt and Kenny Stahl declare that they have no conflict of interest

C. G. Frankær · A. C. Raffalt · K. Stahl (✉)
Department of Chemistry, Technical University of Denmark, Kemitorvet 207, 2800 Kongens Lyngby, Denmark
e-mail: kenny@kemi.dtu.dk

Introduction

Strontium has a high affinity for bone and is readily incorporated into bone matrix. Administration of strontium to rodents, dogs, monkeys, and humans has been shown to result in increased bone strength and reduction of fracture risks [1–5]. Accordingly two organic salts of strontium, strontium ranelate (SrR) and strontium malonate (SrM), have been developed as new drugs for the treatment of osteoporosis, a major worldwide health problem affecting an estimated 75 million people in Europe, the United States, and Japan. The disease is characterized by an imbalance between the rates of bone resorption and bone formation, leading to a reduced bone mass and increased risk of fractures. Clinical trials have shown that SrR reduces the risk of vertebral and nonvertebral fractures in women with osteoporosis [1–3]. In experimental studies, SrR treatment has been shown to prevent loss of trabecular bone strength [4] and to improve fracture healing in estrogen-deficient rats [5]. Ammann et al. [6] reported that 2 years of treatment with SrR increased trabecular and cortical bone mass and bone strength in healthy rodents. Similar results have been obtained in animal studies with SrM [7]. The effects of SrR on osteoporosis have recently been summarized in a review [8].

One of the key factors to understand the effect of strontium as a drug for the treatment and prevention of osteoporosis is the mechanism by which it is incorporated into bone matrix during treatment [9]. However, this mechanism remains unknown. Bone tissue is a nanocomposite material with a hierarchical structure primarily consisting of hydroxyapatite (HA) and collagen, with bone cells and fluid filling up the gaps within and between the collagen fibrils and fibers. Bone apatite has the ability to interact with elements other than Ca, due to the fact that the mineral when present in bone is poorly

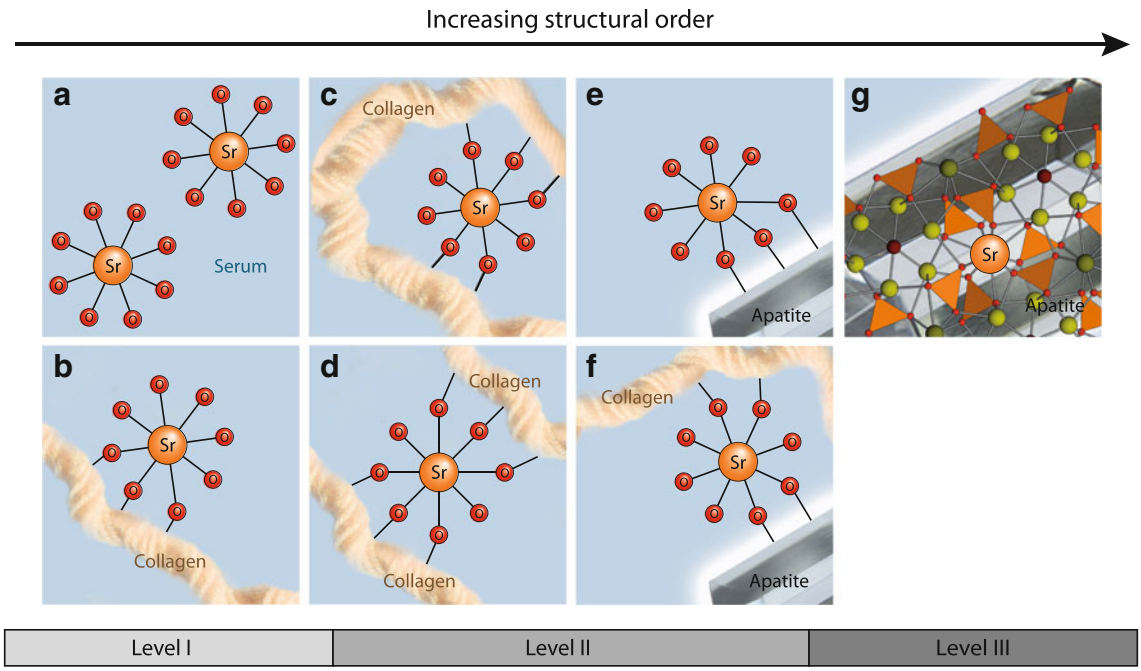

Fig. 1 Possible locations of Sr in bone tissue: **a** in serum, **b** adsorbed to the surface of collagen, **c** intrafibrillar cross-linking of a collagen polymer, **d** interfibrillar cross-linking of collagen polymers, **e** adsorbed to the surface of HA nanocrystals by binding to the hydrated layer, **f** ionic coupling of collagen polymer to HA surface, **g** full incorporation into the apatite structure

crystallized, Ca-deficient, and nonstoichiometric [10]. Also, nonapatitic phosphate species may be present. A list of apatitic as well as nonapatitic phosphates is summarized by Wopenka and Pasteris [11].

Considering the physicochemical properties of these components, possible pathways of incorporation of ions have been suggested [12, 13], and plausible locations of strontium with different levels of structural order have been summarized [10, 14]. Figure 1 summarizes the possible locations of strontium with increasing structural order. The less structurally ordered Sr^{2+} cations may be present in the serum in the bones (Fig. 1a) or adsorbed on the surface of collagen (Fig. 1b, level I), in which Sr^{2+} will be surrounded by an inner coordination sphere consisting of oxygen atoms. The Sr^{2+} cations may then be absorbed in collagen by intra- as well as interfibrillar cross-linking (Fig. 1c, d, respectively), which binds the collagen fibers together. Sr^{2+} cations may also bind to the hydrated layer of poorly crystalline Ca phosphates (Fig. 1e) or link the collagen to the surface of an HA crystal by ionic coupling (Fig. 1f, level II). These interactions are known as "sacrificial bonds" and impact on the mechanical properties of the material [15]. Furthermore, the interaction with collagen is suggested to play an important role as a nucleation site for HA [16]. Finally, Sr^{2+} cations may be incorporated into the calcium HA (CaHA, level III) where they are highly ordered (Fig. 1g). Determining the localization of Sr^{2+} cations may help to clarify suggested hypotheses about strontium uptake in physiological calcifications.

In the present work we studied the localization of strontium incorporated into the bones of dogs treated with SrM. The dogs were treated by daily oral administration of up to 1,000 mg SrM/kg body weight for up to 52 weeks. Sr content in the bone matrix was determined by inductively coupled plasma mass spectrometry (ICP-MS), and the bones were analyzed by X-ray powder diffraction (XRPD) and X-ray absorption spectroscopy (XAS). XAS is well suited for studying the local environment of a specific element present in small concentrations, and the method has previously been used for characterization of calcifications and apatite structures, often in combination with other complementary techniques such as diffraction and vibrational spectroscopy [17].

The first XAS studies of bone, carried out on the Ca *K*-edge, revealed a higher disorder of the calcium ion environment present in bones compared to that of a synthetic, prepared CaHA sample [18, 19] and that the average calcium location is best described by a partially crystalline hydroxyapatite [20–22]. Later, an extended X-ray absorption fine structure (EXAFS) study on human bone involving different bone types again suggested that calcium is present as disordered HA and that its chemical environment remains the same in all the analyzed bone types [23].

In these studies the disorder of calcium is included in the EXAFS models as higher displacement factors, which cover both static and thermal (Debye–Waller) disorder. The static disorder among Ca ions is highest in bone tissue containing carbonates, which reduces the crystallite size,

whereby a larger fraction of nonapatitic calcium may be present in the gaps between the HA crystallites. Also, the bone resorption process is closely related to the degree of disorder in the CaHA and thereby closely related to the composition of the mineral phase [23].

XAS has also been used to study disordered CaHA nanocrystals [24] and calcium phosphates in nonapatitic environments, e.g., dicalcium phosphate, tricalcium phosphate, and octacalcium phosphate [25]. The subtle features in the X-ray absorption near edge structures (XANES) allowed discrimination between the different species, which were found to exist in poorly crystalline synthetic apatites. A recent study demonstrated that XANES could be used to assess and characterize calcium phosphates in human osteoarthritic articular cartilage [26]. Furthermore, XAS has been used to study the insertion of other elements in the HA structure, e.g., Cd [27], Ga [28], Zn [29], Ba and Pb [30].

As the description of static disorder among calcium or strontium in HAs may be insufficient by the classical shell models used for EXAFS interpretation, we suggest a new approach in which XAS spectra are analyzed by a linear combination of spectra of selected components present in the bone sample. This allows us to estimate the relative distribution of strontium in the different bone components.

Materials and Methods

Three reference compounds representing the Sr coordination in each of the three phases in the incorporation hypothesis described above were used in this study. A 0.3 M solution of $SrHPO_4$ was made by dissolving $SrHPO_4$ in 10 % phosphoric acid. Sr-soaked collagen was prepared from a suspension containing 35 mg/mL Bornstein & Traub type I collagen (Sigma, St. Louis, MO; C9879) and 0.1 M $SrCl_2$ $6H_2O$ in isotonic NaCl solution (0.9 %). The collagen was soaked for 4 weeks under agitation, recovered by filtration, and washed six times with isotonic NaCl solution. CaHA with approximately 5 % (w/w) Ca substituted by Sr was prepared by modifying the synthesis of pure CaHA reported by Kumta et al. [31] to include $SrCl_2$ as a starting material in an amount corresponding to 5 % (w/w) Sr substitution of Ca. The Sr concentration in the apatite was confirmed using ICP-MS and further analyzed by XRPD.

Animal bones were obtained from a toxicological study of SrM, which is being developed by Osteologix (Dublin, Ireland) as an antiosteoporotic drug. The in-life part of the study was conducted by LAB Scantox (Ejby, Denmark) under GLP conditions, and all ethical guidelines were followed during the study. Bone samples were obtained using an additional protocol for sampling in parallel to the sampling performed to analyze the bones by certified laboratories. SrM was administrated as a liquid suspension and given to the dogs by oral gavage once a day. Doses are listed in Table 1.

Table 1 Doses and content of Sr in the bone samples analyzed

	Sample	SrM dose (mg/kg/day)	Sr concentration (mg/g)
Femur, 4 weeks, low dose	59,147-7	300	5.7 ± 0.5
Femur, 4 weeks, high dose	59,147-15	1,000	10.4 ± 1.6
Calvaria, 52 weeks, low dose	62,346-16	100	16.2 ± 0.2
Calvaria, 52 weeks, high dose	62,346-25	1,000	36.7 ± 2.0

Femur (thigh) bones and calvariae (skull caps) were dissected from beagle dogs treated with SrM for 4 and 52 weeks, respectively. Calvarial biopsies were sampled using a Rochester Bone Biopsy Kit (i.d. 7 mm; Medical Innovations, Rochester, MN). Adhering soft tissue was removed using a scalpel, and the bones were cleaned with hydrogen peroxide, ethanol, and ultrapure water.

ICP-MS

Calverial biopsies were dried (2 h, 110 °C), dissolved by microwave-assisted acid digestion [approximately 0.5 g bone; 5 mL 65 % HNO_3, Merck Suprapur (Merck, Darmstadt, Germany); 0.5 mL 30 % HCl, Merck Suprapur; 3 mL 35 % H_2O_2 (Riedel de Haën, Seelze, Germany)] in an Anton-Paar Multiwave 3,000 microwave oven, and diluted to appropriate Sr concentrations with ultrapure water (18.2 MΩ cm, Milli-Q Plus; Millipore, Billerica, MA). Calvarial Sr concentrations were determined by ICP-MS using a Perkin-Elmer (Waltham, MA) ELAN 6,000 equipped with a cross-flow nebulizer. Femur samples were pretreated and analyzed as described [32]. Treatment dose, treatment time, and bone Sr concentrations are summarized in Table 1.

XRPD

XRPD data for Sr-doped CaHA were collected on a Huber (Rimsting, Germany) G670 diffractometer using Cu $K\alpha_1$ radiation ($\lambda = 1.5406$ Å) for 30 min at room temperature. XRPD data for bone samples were collected at MAX-lab beam line I711 (Lund, Sweden) on a Huber G670 diffractometer using synchrotron radiation with a wavelength $\lambda = 1.2641$ Å. Data were collected on the bone samples for 20 min at 323 K. The diffraction patterns of the bone samples were part of an experiment where the organic bone components were pyrolyzed and the apatite recrystallized by ramping the temperature to 1,073 K.

Table 2 Number of spectra and data collection ranges for the samples

	Number of spectra	Data collection range (eV)
Sr-phosphate solution	2	15,955–17,065
Sr-soaked collagen	3	15,955–16,600
Sr-doped CaHA	2	15,955–17,065
Femur, 4 weeks, low dose	3	15,955–16,900
Femur, 4 weeks, high dose	3	15,955–17,050
Calvaria, 52 weeks, low dose	3	15,955–16,900
Calvaria, 52 weeks, high dose	3	15,955–17,050

XRPD data were subsequently analyzed by the Rietveld method [33], in which the peak shapes were modeled by the Voigt function. The crystallite sizes of HA were determined from full width at half-maximum of the Lorentzian contribution, whereas the peak broadening originating from the experimental setup was determined by the gaussian contribution and described by the Cagliotti parameters, which were held constant at values determined from a silicon standard.

XAS

For XAS experiments the Sr phosphate solution and the collagen were mounted in a 1-mm-thick sample holder for XAS, whereas the powder was pressed in tablets of approximately 1 mm thickness. Bone samples were ground, pressed into tablets, and mounted on the sample holder of the cryostat used. Sr *K*-edge X-ray absorption spectra were recorded on beam line I811 at MAX-lab, using a Si(311) double-crystal monochromator detuned 30 % at 16,750 eV (further specifications can be found in Carlson et al. [34]). Fluorescence data were collected at 100 K using a liquid nitrogen cryostat (Optistat, Oxford Instruments, High Wycombe, UK) using a passive implanted planar silicon detector (PD-5000, Canberra Industries, CT, USA). Two or three spectra were collected for each sample. The data collection ranges are specified in Table 2, and the data collection times were as follows: pre-edge data (150–30 eV before the edge) were collected in steps of 5 eV for 1 s, the edge (from 30 eV before to 30 eV beyond the edge) in steps of 0.3 eV for 1 s, and the EXAFS (from 30 eV beyond the edge) in steps of 0.05/Å for 1–15 s. No degradation or radiation damage of the samples was observed.

In general, the concentration of strontium in the analyzed bone samples is very high compared with the natural levels of 0.07–0.13 mg/g found in the corresponding placebo-treated animals. The more than 50 times higher concentrations present in these samples provided XAS spectra with good signal-to-noise ratios. Averaging, subtraction of background, and normalization were carried out using WinXAS [35]. All spectra were energy-calibrated using a simultaneously collected spectrum of strontium chloride hexahydrate for which the main edge inflection point was assigned to 16,109.8 eV [36].

XAS spectra for the bone samples were modeled by a linear combination of XAS spectra of three representative reference compounds (SrHA, Sr-soaked collagen, and Sr phosphate solution). The EXAFS spectra $\chi(k)$ were fitted with the linear combination fit procedure included in ATHENA [37, 38], which uses a function of the type

$$\chi_{\mathrm{Bone}}(k) = [a_{\mathrm{HA}} \cdot \chi_{\mathrm{HA}}(k)] + [a_{\mathrm{Col}} \cdot \chi_{\mathrm{Col}}(k)] + [a_{\mathrm{Sol}} \cdot \chi_{\mathrm{Sol}}(k)], \quad (1)$$

in which $\chi_{\mathrm{i}}(k)$ and a_{i} are the EXAFS function and the fraction of reference compound i, respectively. The coefficients a_i were determined by a least squares procedure and forced to sum up to 1. The quality of the fit was evaluated by an R factor given as

$$R_{\mathrm{exafs}} = \frac{\sum[(\chi_{\mathrm{Exp}}(k) - \chi_{\mathrm{Bone}}(k))^2]}{\sum[(\chi_{\mathrm{Exp}}(k))^2]}\ 100\ \%. \quad (2)$$

Results

Administration of SrM to beagle dogs was generally well tolerated. Dogs were treated for 4 or 52 weeks with doses up to 1,000 mg SrM/kg body weight/day. These doses are substantially above the suggested human Sr dose used in clinical studies of SrR and SrM. After completion of the study, the animals were put to death and tissues, including bone, obtained for analysis.

The X-ray powder diffractograms for calvaria, femur bone, and 5 % Sr-doped CaHA are shown in Fig. 2. The powder patterns collected at the synchrotron have been converted to Cu $K\alpha_1$ radiation ($\lambda = 1.5406$ Å) after the Rietveld refinements. Common for all samples is that they consist of HA, albeit with different crystallite size, which is seen as different peak broadenings.

The occupancies of Sr were refined, and the Voigt particle sizes of the HA were determined for the bone samples by Rietveld refinements. The results are summarized in Table 3. It should be noted that due to crystal defects the sizes determined are the coherence lengths and the crystallite sizes may be somewhat underestimated.

In the bone samples Sr incorporations of 6–8 % were observed, with a slightly higher incorporation in the calvaria compared to the femur sample. This observation is in accordance with the results from a study of Sr distribution among different bones in rats treated with SrR [39]. Heating the bone sample to high temperatures provides recrystallization of the HA, where larger particles are formed. This is seen in the powder pattern as decreased

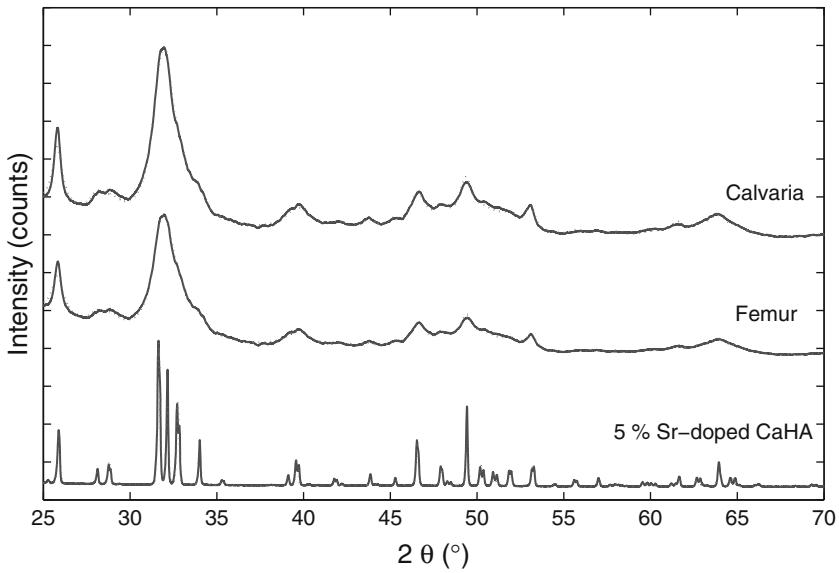

Fig. 2 XRPD patterns of bone samples and Sr-doped CaHA. From *top* calvaria, femur bone, and 5 % Sr-doped CaHA. Calculated patterns from the Rietveld analysis are included and shown as *dotted lines*. Patterns collected at $\lambda = 1.2641$ Å are converted to Cu $K\alpha_1$ radiation $\lambda = 1.5406$ Å

Table 3 Unit cell parameters, particle sizes, and occupancies for HA as determined by Rietveld refinement

	Femur, 4 weeks, high dose	Calvaria, 52 weeks, high dose	5 % Sr-doped HA
Unit cell parameters			
a (Å)	9.441 (1)	9.441 (1)	9.4650 (4)
c (Å)	6.8900 (3)	6.8974 (3)	6.8785 (2)
V (Å^3)	531.8 (2)	532.7 (1)	533.7 (1)
Voigt particle sizes (nm)			
//a	6.1	6.0	
//c	12.0	13.8	
No. of total Ca/Sr sites pr. particle	7,270	8,065	
No. of surface Ca/Sr-sites pr. particle	2,668	2,943	
x_{surf} (%)	37	36	
Occupancies of Sr			
Ca/Sr site(I)	0.065 (3)	0.085 (3)	0.048 (4)
Ca/Sr site(II)	0.060 (2)	0.073 (2)	0.053 (5)
Sr(I):Sr(II)	0.72 (4)	0.78 (3)	0.60 (8)

peak broadening, which may allow a better determination of the Sr content. Therefore, an attempt to verify the Sr content in the femur sample after pyrolysis was carried out. In the following Rietveld analysis Voigt particle sizes of 85 × 100 nm were observed, but more surprisingly the unit cell parameters determined from the analysis revealed that Sr is not incorporated in the apatite after the recrystallization; thus, the verification was abandoned.

Sr atoms located on the surface of the crystallite might be considered as partly disordered. The fraction of apatitic M^{2+} sites (M = Ca or Sr) located on the surface, x_{surf}, is listed in Table 3 and was estimated by assuming that half of the M atoms present in a unit cell located on the surface of a particle are partly disordered:

$$x_{surf} = \frac{0.5 \times \text{Unit cells on surface}}{\text{Total number of unit cells}} \times 100\,\% = \frac{0.5 \times (2 \times N_a^2 + 4 \times N_a N_c)}{N_a^2 N_c} \times 100\,\% \quad (3)$$

where N_a and N_c are the number of unit cells along the crystallographic a- and c-axes, respectively. Introducing $N_a = 6.5$ and $N_c = 17.4$, $x_{surf} = 37$ %. For the particle sizes reported here, it is seen that around one-third of the M^{2+} atoms are located on the surface of the crystallite.

XANES spectra for all bone samples and the three reference compounds are shown in Fig. 3. In the XANES region, the bone samples are very similar. For SrHA a small feature is clearly observed at 16,135 eV, which could

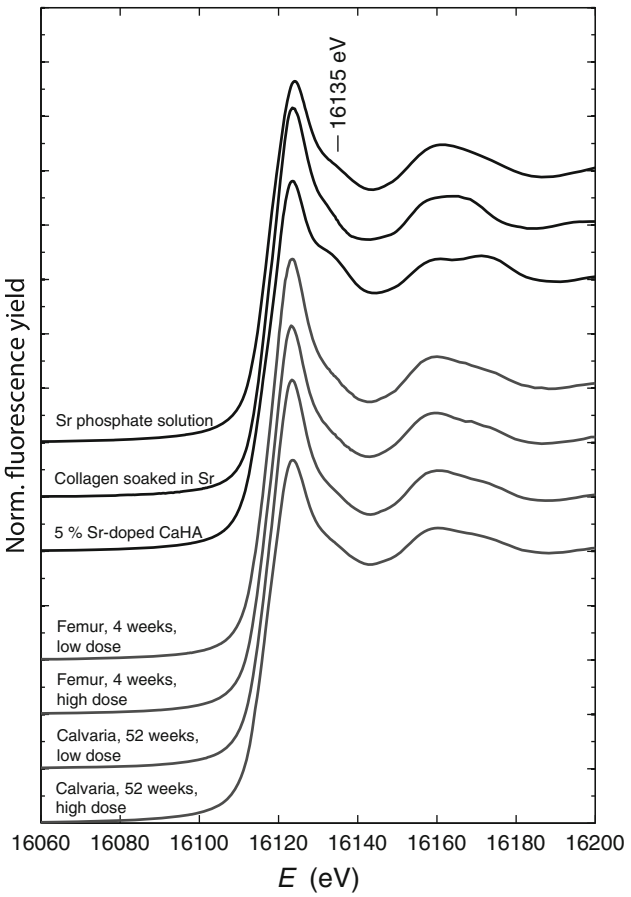

Fig. 3 XANES spectra collected at the Sr *K*-edge of Sr-treated bone samples and reference compounds

be assigned to outer coordination spheres [14] and thereby verify the incorporation of Sr^{2+} cations in apatite. The EXAFS of the three reference compounds are very different. For Sr^{2+} cations in solution only the inner coordination sphere is observed, whereas for SrHA and Sr-soaked collagen several coordination spheres are observed, implying that the Sr^{2+} cations are coordinated to and inserted in the solid matrix. The extracted EXAFS and the radial electron density distributions are shown in (Fig. 4a, b, respectively). It is clear that strontium in the bone samples is partly incorporated in the apatite structure. Likewise, it is also clear that the Sr^{2+} cations are not exclusively present as apatite. As XAS probes the average localization of the absorbing atom type, the XAS spectra for the bone samples were modeled by a linear combination of XAS spectra of the three representative reference compounds using Eq. 1. The coefficients a_i describing the distribution of strontium coordination and the residuals are listed in Table 4.

The fitted EXAFS spectra are shown in Fig. 4a as dashed lines.

Discussion

The localization of strontium in physiological calcifications depends on how strontium is inserted into bone matrix. The hierarchical structure of bone and its many different components make the material highly inhomogeneous and provide many different coordination sites for strontium. In general, the suggested plausible Sr sites agree that the positively charged strontium ions have a high affinity for coordination to oxygen atoms, which are available in high amounts in the bone components.

In this study, presence of Sr^{2+} cations in bone fluid was represented by an aqueous solution of Sr^{2+}. As only one coordination sphere is clearly visible in the XAS spectrum from the Sr phosphate solution, a high static and/or kinetic disorder among the outer coordination shells is well imitated by this sample. Further analysis of this spectrum reveals a strontium coordination number of 8.1(7) oxygen atoms with a distance of 2.600(4) Å and a Debye–Waller factor of $\sigma^2 = 0.009(1)$, which perfectly match the Sr–O distance of 2.57 Å and coordination number of eight reported in an EXAFS study on solubilized Sr^{2+} cations performed at 298 K [40].

The structural order increases as strontium is inserted into collagen and HA. This is seen for the Sr-soaked collagen as the outer coordination spheres become visible in the radial electron density distribution and in the HA, in which the structural order is even higher, and the electron density shells become more intense and better resolved.

The HA present in the bone samples is poorly crystalline, as seen from the peak broadening in the XRPD patterns; and the HA nanocrystals were determined to be around 10 nm from the Rietveld refinement, with an elongation in the crystallographic *c* direction, which is comparable to crystallite sizes reported elsewhere as determined by XRPD [23] and transmission electron microscopy [41, 42]. In these studies the crystallite sizes range from a few nanometers up to 50 nm depending on bone type.

The XAS fitting results clearly demonstrated that at least 35–45 % of the total strontium content is incorporated into CaHA. Furthermore, taking into account the disordered Sr atoms located on the surface of the HA crystals, the fraction of strontium which is either inserted into or coordinated to the surface of the apatite may increase. In apatite, the divalent cations can occupy two crystallographically different sites, M(I) and M(II) present in an M(I):M(II) ratio of 2:3 [43]. A preferential occupation among the two crystallographic sites upon substitution of Ca^{2+} by other cations depends on the size of the cation [44]. Sr^{2+} preferentially occupies the M(I) site when present at low doping levels (<1 atom %), whereas an ideal and equal distribution, Sr^{2+}(I):Sr^{2+}(II) = 0.66, is observed at doping

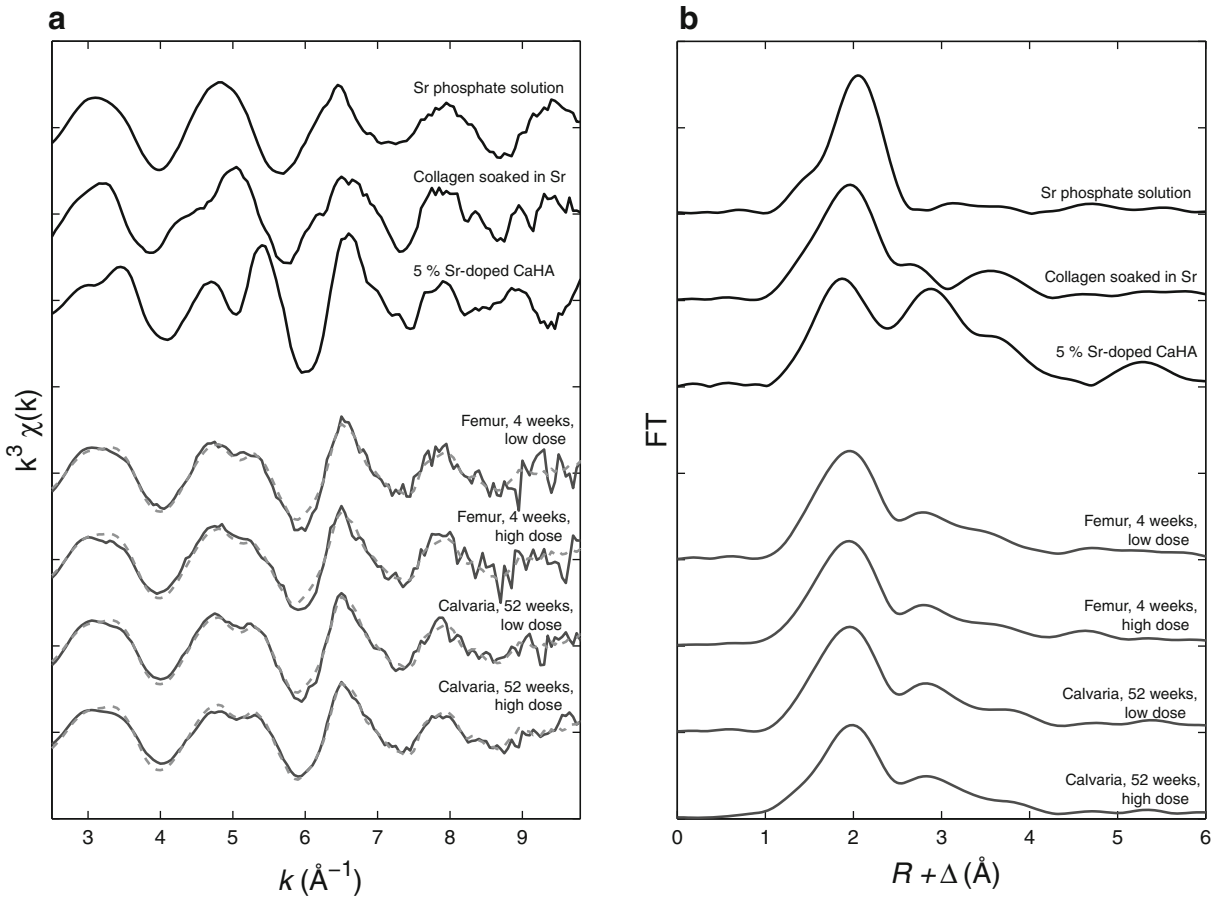

Fig. 4 **a** Extracted and k^3-weighted EXAFS function $k^3\chi(k)$. The bone spectra are fitted to a *dashed curve* with a linear combination of EXAFS spectra for SrHA, Sr-soaked collagen, and Sr^{2+} cations in solution. The distribution coefficients are listed in Table 3. **b** The modulus of its Fourier transform giving the radial electron density distribution

Table 4 Relative distribution of strontium localization in bone samples as determined by XAS

	a_{HA}	a_{Col}	a_{Sol}	R_{exafs} (%)
Femur, 4 weeks, low dose	0.44 (2)	0.15 (4)	0.41 (5)	4.9
Femur, 4 weeks, high dose	0.36 (2)	0.18 (5)	0.46 (5)	6.7
Calvaria, 52 weeks, low dose	0.44 (2)	0.17 (4)	0.39 (4)	4.0
Calvaria, 52 weeks, high dose	0.45 (1)	0.21 (3)	0.34 (3)	3.7

Distribution coefficients are given as fractions a_i representing the fraction of strontium incorporated in hydroxyapatite, coordinated to collagen, or present in solution. Standard deviations determined from the least squares fit are given in parentheses

levels around 5 % [45, 46]. For a higher degree of Sr substitutions the Sr^{2+} preferably occupies the M(II) site [47]. An approximately equal distribution among the two sites, Sr^{2+}(I):Sr^{2+}(II) ranging from 0.60 to 0.78, was confirmed by a Rietveld refinement for the 5 % Sr-doped HA as well as the bone samples analyzed in this study. Using XAS, demonstration of a possible preference toward one of the sites in the bone samples is, however, beyond the information level of the XAS data presented here. Likewise, the influence of vacancies and defects in the apatite lattice is beyond the level of what can be detected by XAS.

XAS is a well-suited method to study the localization of Sr^{2+} cations in bone tissue as it is element-specific and very sensitive to small concentrations. In analogy to earlier XAS studies of the calcium environment in bone minerals [18–23], this study clearly demonstrates that Sr occupies different and highly disordered sites. The approach by which the EXAFS data are treated is, however, different. In the common shell approach static as well as thermal (Debye–Waller) disorder are modeled as higher displacement factors. An attempt to model the EXAFS data presented here by the shell approach was carried out but

abandoned as it resulted in chemically unreasonable models, in which many of the shells were either merged or omitted.

Using a compositional approach for analysis of the EXAFS spectra, where a linear combination of experimental spectra of selected components present in bone is fitted to the data, allows for a quantitative estimate of the disorder among the strontium present in bone and further offers a way to estimate the relative distribution of strontium in the different bone components, which is not possible by the shell approach. It was possible to fit a linear combination of only two components (SrHA and Sr in solution) to the EXAFS, but including all three components gave a significantly better fit (Table 4). Generally, it is evident that strontium occupies highly disordered sites in which only the first coordination shell is visible by XAS and that the distance to this inner coordination sphere resembles the bond lengths of Sr–O. Such sites are better described by the aqueous Sr^{2+} cations in solution rather than Sr-soaked collagen and may account for at least 30–50 % of the total strontium content.

This study clearly demonstrates that strontium is inserted into different bone matrix compartments with different levels of structural order. The fact that Sr^{2+} has a larger ionic radius than Ca^{2+} (1.26 vs. 1.12 Å for eight coordinated species) means that it has a larger range of coordination with the ability to reach further than Ca^{2+} and thereby increase the possibility of being involved in cross-linking of collagen, as well as ionic coupling between apatite and collagen (see Fig. 1). This is in line with previous in vivo studies where increased bone strength has been observed after treatment with strontium ranelate [48] as well as in vitro studies of bone soaked in solutions of $SrCl_2$ where insertion of Sr^{2+} caused an improved microarchitecture, providing a stiffer, harder, and tougher material [49].

The result from the EXAFS analysis did not show any significant differences in the relative distribution of strontium in the four bone samples. Thus, while the dose levels and treatment time highly influence the bone strontium concentrations, the relative amounts of strontium incorporated into CaHA seem to be independent of these factors. It is understandable that the relative fraction of Sr incorporated into CaHA seems to be independent of strontium dose as there may be an upper level of saturation. More surprising is that the relative fraction of Sr incorporated into HA seems to be independent of treatment time and/or bone type. The replacement of calcium ions in HA is a slow process compared to the time strontium ions in solution around HA crystals come to equilibrium with daily dosing. However, the actual time it will take the entire system to reach equilibrium will depend on the size of the HA nanocrystals. The sizes of the HA crystals, as estimated from the Rietveld refinement, were in the range 6–14 nm, which is small enough so that substitution of calcium with strontium can occur faster and equilibrium conditions can be reached within 4 weeks, resulting in incorporation of strontium into fully ordered apatite sites.

Conclusion

The study shows that even very high levels of strontium administration, several magnitudes beyond the doses used in human clinical interventions, will result in incorporation of Sr into the bone matrix in a similar way as low-dose administration. From this study of bone samples from dogs treated with SrM, around 35–45 % of the strontium present is incorporated into CaHA by substitution of some of the calcium ions and localized in highly ordered sites in the interior of these crystals. At least 30 % is located at sites with a high structural disorder similar to Sr^{2+} in solution. The remaining strontium is either present on the surface of HA crystals or absorbed in collagen, in which it obtains a higher structural order than when present in solution but less order than when it is incorporated into CaHA. These observations strongly support the insertion of strontium into different bone components with different levels of structural order.

Analyzing the EXAFS spectra by fitting a linear combination of spectra of selected components present in bone resulted in a new compositional model. This approach allowed the relative distribution of strontium in the different bone components to be estimated, in contrast to the common shell models. In this study, the distribution of strontium among the different components seems to be independent of treatment period and dose level.

Acknowledgments We are grateful to Katarina Norén for assistance with data collection on beam line I811 at MAX-lab. The donation of bone samples by Stephan Christgau of Osteologix is gratefully acknowledged.

References

1. Meunier PJ, Roux C, Seeman E, Ortolani S, Badurski JE, Spector TD, Cannata J, Balogh A, Lemmel EM, Pors-Nielsen S, Rizzoli R, Genant HK, Reginster JY (2004) The effects of strontium ranelate on the risk of vertebral fracture in women with postmenopausal osteoporosis. N Engl J Med 350:459–468
2. Reginster JY, Felsenberg D, Boonen S, Diez-Perez A, Rizzoli R, Brandi ML, Spector TD, Brixen K, Goemaere S, Cormier C, Balogh A, Delmas PD, Meunier PJ (2008) Effects of long-term strontium ranelate treatment on the risk of nonvertebral and vertebral fractures in postmenopausal osteoporosis: results of a five-year, randomized, placebo-controlled trial. Arthritis Rheum 58:1687–1695
3. Reginster JY, Seeman E, De Vernejoul MC, Adami S, Compston J, Phenekos C, Devogelaer JP, Curiel MD, Sawicki A, Goemaere S, Sorensen OH, Felsenberg D, Meunier PJ (2005) Strontium

ranelate reduces the risk of nonvertebral fractures in postmenopausal women with osteoporosis: treatment of peripheral osteoporosis (TROPOS) study. J Clin Endocrinol Metab 90:2816–2822
4. Bain SD, Jerome C, Shen V, Dupin-Roger I, Ammann P (2009) Strontium ranelate improves bone strength in ovariectomized rat by positively influencing bone resistance determinants. Osteoporos Int 20:1417–1428
5. Ozturan KE, Demir B, Yucel I, Cakıcı H, Yilmaz F, Haberal A (2011) Effect of strontium ranelate on fracture healing in the osteoporotic rats. J Orthop Res 29:138–142
6. Ammann P, Shen V, Robin B, Mauras Y, Bonjour JP, Rizzoli R (2004) Strontium ranelate improves bone resistance by increasing bone mass and improving architecture in intact female rats. J Bone Miner Res 19:2012–2020
7. Raffalt AC (2011) Effects of strontium malonate (NB S101) on the compositional, structural and biomechanical properties of calcified tissues in rats and dogs. Dissertation, Technical University of Denmark
8. Marie PJ, Felsenberg D, Brandi ML (2011) How strontium ranelate, via opposite effects on bone resorption and formation, prevents osteoporosis. Osteoporos Int 22:1659–1667
9. Li C, Paris O, Siegel S, Roschger P, Paschalis EP, Klaushofer K, Fratzl P (2010) Strontium is incorporated into mineral crystals only in newly formed bone during strontium ranelate treatment. J Bone Miner Res 25:968–975
10. Bazin D, Daudon M, Combes C, Rey C (2012) Characterization and some physicochemical aspects of pathological microcalcifications. Chem Rev 112:5092–5120
11. Wopenka B, Pasteris JD (2005) A mineralogical perspective on the apatite in bone. Mater Sci Eng, C 25:131–143
12. Rey C, Combes C, Drouet C, Sfihi H, Barroug A (2007) Physicochemical properties of nanocrystalline apatites: implications for biominerals and biomaterials. Mater Sci Eng, C 27:198–205
13. Cazalbou S, Eichert D, Drouet C, Combes C, Rey C (2004) Biological mineralisations based on calcium phosphate. Compte Rendu Palevol 3:563–572
14. Bazin D, Daudon M, Chappard C, Rehr JJ, Thiaudière D, Reguer S (2011) The status of strontium in biological apatites: an XANES investigation. J Synchrotron Rad 18:912–918
15. Fantner GE, Hassenkam T, Kindt JH, Weaver JC, Birkedal H, Pechenik L, Cutroni JA, Cidade GAG, Stucky GD, Morse DE, Hansma PK (2005) Sacrificial bonds and hidden length dissipate energy as mineralized fibrils separate during bone fracture. Nat Mater 4:612–616
16. Nudelman F, Pieterse K, George A, Bomans PHH, Freidrich H, Brylka LJ, Hilbers PAJ, With G, Sommerdijk NAJM (2010) The role of collagen in bone apatite formation in presence of hydroxyapatite nucleation inhibitors. Nat Mater 9:1004–1009
17. Bazin D, Chappard C, Combes C, Carpentier X, Rouzière S, André G, Matzen G, Allix M, Thiaudière D, Reguer S, Jungers P, Daudon M (2009) Diffraction techniques and vibrational spectroscopy opportunities to characterise bones. Osteoporos Int 20:1065–1075
18. Miller RM, Hukins DWL, Hasnain SS, Lagarde P (1981) Extended X-ray absorption fine structure EXAFS studies of the calcium ion environment in bone mineral and related calcium phosphates. Biochem Biophys Res Commun 99:102–106
19. Binsted N, Hasnain SS, Hukins DWL (1982) Developmental changes in bone mineral structure demonstrated by extended X-ray absorption fine structure EXAFS spectroscopy. Biochem Biophys Res Commun 107:89–92
20. Harries JE, Hukins DWL, Hasnain SS (1986) Analysis of the EXAFS spectrum of hydroxyapatite. J Phys C 19:6859–6872
21. Harries JE, Hukins DWL, Holt C, Hasnain SS (1987) Conversion of amorphous calcium phosphate into hydroxyapatite investigated by EXAFS spectroscopy. J Cryst Growth 84:563–570
22. Harries JE, Hukins DWL, Hasnain SS (1988) Calcium environment in bone mineral determined by EXAFS spectroscopy. Calcif Tissue Int 43:250–253
23. Peters F, Schwarz K, Epple M (2000) The structure of bone studied with synchrotron X-ray diffraction, X-ray absorption spectroscopy and thermal analysis. Thermochim Acta 361: 131–138
24. Liou S-C, Chen S-Y, Lee H-Y, Bow J-S (2004) Structural characterization of nanosized calcium deficient apatite powders. Biomaterials 25:189–196
25. Eichert D, Salomé M, Banu M, Susini J, Rey C (2005) Preliminary characterization of calcium chemical environment in apatitic and non-apatitic calcium phosphates of biological interest by X-ray absorption spectroscopy. Spectrochim Acta B 60: 850–858
26. Nguyen C, Ea HK, Thiaudière D, Reguer S, Hannouche D, Daudon M, Lioté F, Bazin D (2011) Calcifications in human osteoarthritic articular cartilage: ex vivo assessment of calcium compounds using XANES spectroscopy. J Synchrotron Rad 18: 475–480
27. Sery A, Manceau A, Greaves GN (1996) Chemical state of Cd in apatite phosphate ores as determined by EXAFS spectroscopy. Am Mineral 81:864–873
28. Korbas M, Rokita E, Meyer-Klaucke W, Ryczek J (2004) Bone tissue incorporates in vitro gallium with a local structure similar to gallium-doped brushite. J Biol Inorg Chem 9:67–76
29. Bazin D, Carpentier X, Brocheriou I, Dorfmuller P, Aubert S, Chappard C, Thiaudière D, Reguer S, Waychunas G, Jungers P, Daudon M (2009) Revisiting the localisation of Zn^{2+} cations sorbed on pathological apatite calcifications made through X-ray absorption spectroscopy. Biochimie 91:1294–1300
30. Sugiyama S, Moriga T, Hayashi H, Moffat JB (2001) Characterization of Ca, Sr, Ba and Pb HAP: X-ray diffraction, photoelectron, EXAFS and MAS NMR spectroscopies. Bull Chem Soc Jpn 74:187–192
31. Kumta PN, Sfeir C, Lee D-H, Olton D, Choi D (2005) Nanostructured calcium phosphates for biomedical applications: novel synthesis and characterization. Acta Biomater 1:65–83
32. Raffalt AC, Andersen JET, Christgau S (2008) Application of inductively coupled plasma-mass spectrometry (ICP-MS) and quality assurance to study the incorporation of strontium into bone, bone marrow, and teeth of dogs after one month of treatment with strontium malonate. Anal Bioanal Chem 391: 2199–2207
33. Rietveld HM (1969) A profile refinement method for nuclear and magnetic structures. J Appl Cryst 2:65–71
34. Carlson S, Clausén M, Gridneva L, Sommarin B, Svensson C (2006) XAFS experiments at beamline I811, MAX-lab synchrotron source, Sweden. J Synchrotron Rad 13:359–364
35. Ressler T (1998) WinXAS: a program for X-ray absorption spectroscopy data analysis under MS-Windows. J Synchrotron Rad 5:118–122
36. Ubgade R, Sarode PR (1987) Study of strontium compounds and minerals by X-ray absorption spectroscopy. Phys Status Solidi A 99:295–301
37. Newville M (2001) IFEFFIT: interactive XAFS analysis and FEFF fitting. J Synchrotron Rad 8:322–324
38. Ravel B, Newville M (2005) ATHENA, ARTEMIS, HEPHAESTUS: data analysis for X-ray absorption spectroscopy using IFEFFIT. J Synchrotron Rad 12:537–541
39. Oliveira JP, Querido W, Caldas RJ, Campos APC, Abraçado LG, Farina M (2012) Strontium is incorporated in different levels into bones and teeth of rats treated with strontium ranelate. Calcif Tissue Int 91:186–195
40. Seward TM, Henderson CMB, Charnock JM, Dreisner T (1999) An EXAFS study of solvation and ion pairing in aqueous

strontium solutions to 300 °C. Geochim Cosmochim Acta 63:2409–2418
41. Plate U, Arnold S, Stratmann U, Weismann HP, Höhling HJ (1998) General principle of ordered apatitic crystal formation in enamel and collagen rich hard tissues. Connect Tissue Res 38:149–157
42. Ziv V, Wagner HD, Weiner S (1996) Microstructure–microhardness relations in parallel-fibered and lamellar bone. Bone 18:417–428
43. Kay MI, A Young R, Posner AS (1964) Crystal structure of hydroxyapatite. Nature 204:1050–1052
44. Tamm T, Peld M (2006) Computational study of cation substitutions in apatites. J Solid State Chem 179:1581–1587
45. Bigi A, Boanini E, Capuccini C, Gazzano M (2007) Strontium-substituted hydroxyapatite nanocrystals. Inorg Chim Acta 360: 1009–1016
46. Terra J, Dourado ER, Eon J-G, Ellis DE, Gonzalez G, Rossi AM (2009) The structure of strontium-doped hydroxyapatite: an experimental and theoretical study. Phys Chem Chem Phys 11:568–577
47. O′Donnell MD, Fredholm Y, de Rouffignac A, Hill RG (2008) Structural analysis of a series of strontium-substituted apatites. Acta Biomater 4:1455–1464
48. Ammann P, Badoud I, Barraud S, Dayer R, Rizzoli R (2007) Strontium ranelate treatment improves trabecular and cortical intrinsic bone tissue quality, a determinant of bone strength. J Bone Miner Res 22:1419–1425
49. Cattani-Lorente M, Rizzoli R, Ammann P (2013) In vitro bone exposure to strontium improves bone material level properties. Acta Biomater 9:7005–7013